Crystal structure, photoluminescence and cathodoluminescence of $Sr_{1-x}Ca_xAl_2O_4$ doped with Eu^{2+}

LIPING YU,[2] DANIEL DEN ENGELSEN,[1] JÜRGEN GOROBEZ,[3]
GEORGE R. FERN,[1] TERRY G. IRELAND,[1,*] [ID] CHRIS FRAMPTON,[1]
AND JACK SILVER[1]

[1]*Centre for Phosphor and Display Materials, Wolfson Centre for Materials Processing, Brunel University London, Uxbridge, Middlesex, UB8 3PH, UK*
[2]*On leave from the College of Chemistry and Chemical Engineering, Hunan Normal University, Changsha, 410081, China*
[3]*On leave from Department of Chemical Engineering, University of Applied Sciences Münster, Stegerwaldstrasse 39, D-48565, Steinfurt, Germany*
*terry.ireland@brunel.ac.uk

Abstract: The crystal structure, photoluminescence and some cathodoluminescent spectra of $Sr_{0.99-x}Ca_xEu_{0.01}Al_2O_4$ (Eu^{2+}) are described. Five different phases have been found: three different monoclinic phases, one hexagonal and one cubic phase. Based on the cathodoluminescence of $SrAl_2O_4:Eu^{2+}$ at low temperature and photoluminescence of $Sr_{1-x}Ca_xAl_2O_4:Eu^{2+}$ at $0 \leq x \leq 0.1$, we consider an alternative explanation for the origin of the 440 nm peak in the low temperature spectrum of $SrAl_2O_4:Eu^{2+}$, namely that it can be attributed to the emission from Eu^{2+} ions situated on the alkaline earth sites of the monoclinic $P2_1/n$ structure that generate the 440 nm emission of $CaAl_2O_4$. However, this alternative hypothesis has been eliminated by XRD analyses of $SrAl_2O_4$ at low temperature.

1. Introduction

As part of an ongoing study on metal aluminate phosphors activated with Eu^{2+} we have investigated the luminescence of the phosphor series $Ba_{1-x}Sr_xAl_2O_4$, $Sr_{1-x}Ca_xAl_2O_4$ and $Ba_{1-x}Ca_xAl_2O_4$ doped with Eu^{2+}. Herein we shall describe the results for $Sr_{1-x}Ca_xAl_2O_4$, the results for $Ba_{1-x}Sr_xAl_2O_4$ and $Ba1_{-x}Ca_xAl_2O_4$ will be published separately. In consequence of their rather high photoluminescence (PL) efficiency the alkaline earth (Ca, Sr or Ba) aluminates doped with Eu^{2+} have been extensively studied [1]. When excited in the near UV, the fluorescence emission colour of $SrAl_2O_4:Eu^{2+}$ is green, that of $CaAl_2O_4:Eu^{2+}$ is blue and that of $BaAl_2O_4:Eu^{2+}$ is cyan [1–7]. This colour variation is due to the sensitivity of the crystal field components of the $4f^65d$ excited state configuration of the Eu^{2+} ion in the three crystal structures.

The synthesis and luminescence properties of $MAl_2O_4:Eu^{2+}$ (M = Ba, Ca, Mg and Sr) phosphor powders were almost simultaneously reported in 1968 by Blasse et al. [2,3] and Palilla et al. [4]. Blasse and Bril reported that the PL efficiency of these phosphors is rather high, whereas the cathodoluminescence (CL) efficiency is only 1-3% [2]. In a study on the optical and electrical properties of $SrAl_2O_4:Eu^{2+}$ in 1971 by Abbruscato [5] it was concluded that the method of excitation of Eu^{2+} under UV- and electron beam excitation is predominantly of the charge transfer type. Abbruscato also found that the luminescence of $SrAl_2O_4:Eu^{2+}$ increased substantially by changing the $SrO:Al_2O_3$ ratio from the stoichiometric value to 5 mol% excess Al_2O_3. As well as having short decay times, the luminescence decay of the Eu^{2+} doped alkaline earth aluminates,

MAl_2O_4:Eu^{2+} (M = Ca, Sr, Ba), can also be adapted using co-activators (particularly Dy^{3+}) to manifest luminescence with very long lifetimes and the same characteristic luminescence in the visible spectrum [7–12] These investigations have led to the widespread use of especially $SrAl_2O_4$:Eu^{2+},Dy^{3+} as a persistent luminescence material.

From the first decade of the last century onwards, alkaline earth aluminates have been intensively studied for their use in cements. These are refractory materials and were traditionally prepared by solid state reactions at high temperature (1200-1600°C) [13,14]. For phosphor applications with Eu^{2+} as dopant, the reactions need to be carried out in reducing atmospheres so that the europium activator is present as the divalent cation [1–7]. $BaAl_2O_4$, $CaAl_2O_4$ and $SrAl_2O_4$ have stuffed tridymite crystal structures, which can be represented as layers of rings of vertex sharing AlO_4 tetrahedra, in which Ba, Ca or Sr respectively occupy tricapped trigonal anti-prismatic cavities. The ideal undistorted structures of MAl_2O_4 (M = Ca, Sr or Ba) at high temperature for $SrAl_2O_4$ and $BaAl_2O_4$ are represented by the $P6_322$ space group [15–18]. At room temperature this ideal structure is distorted, either to monoclinic structures as in the case of $CaAl_2O_4$ and $SrAl_2O_4$, or to a lower symmetry hexagonal structure ($P6_3$) for $BaAl_2O_4$. $SrAl_2O_4$ has a monoclinic crystal structure at ambient temperature and pressure [15], the hexagonal structure is the stable phase at a temperature > 675°C, then it is again monoclinic at even higher temperatures [16]. $BaAl_2O_4$ has attracted special attention due to its phase change from the ferroelectric (space group $P6_3$) to the paraelectric state (space group $P6_322$), which takes place at about 400 K [19,20]. Aitasalo et al. [21] reported the existence of hexagonal $CaAl_2O_4$:Eu^{2+}, which can only be prepared by a sol-gel method.

As introduced above, the efficient PL of the alkaline earth aluminates doped with Eu^{2+} has stimulated much research, especially for aluminates that contain Sr [2–12,22–27]. The primary reason for the interest in $SrAl_2O_4$:Eu^{2+} is its rather intense green luminescence compared to the less bright luminescence of $CaAl_2O_4$:Eu^{2+} and $BaAl_2O4$:Eu^{2+}. The PL spectrum of $SrAl_2O_4$:Eu^{2+} at low temperature has attracted much attention since the assignment of the high energy band at 440 nm of the emission spectrum by Poort et al. [6]. There are two suggested explanations to account for the origin of this high energy band; the first is that the high energy peak (at 440 nm) can be assigned to an Eu^{2+} ion at one of the two Sr sites in monoclinic $SrAl_2O_4$ [6,24,26], while the main emission band at 520 nm is attributed to Eu^{2+} at the other Sr site. This explanation ignores the asymmetric character of this emission band. The second explanation acknowledges the asymmetric character of the main emission band and concludes that it consists of two components, which are attributed to the emission of Eu^{2+} ions at the two Sr sites [25,28]. Clabau et al. [25] assumed that the high energy peak at 440 nm arises from charge transfer from oxygen to residual Eu^{3+} that takes place upon UV irradiation and is associated with hole trapping at Sr^{2+} vacancies.

Figure 1 presents the composition diagram of the ternary systems CaO-SrO-Al_2O_3, which is largely based on the data presented in Shuklás thesis [29], the literature mentioned therein and the work of Ptáček [13] and Ropp [14]. In Fig. 1 the notation of the cement chemistry has been adopted, in which A stands for Al_2O_3, B stands for BaO, C stands for CaO and S stands for SrO. These abbreviations will also be used in this paper. The red lines SA-CA and BA-SA indicate the compositions that were investigated and are described herein. The compounds in Fig. 1 emphasized with a red mark that are not positioned on one of the red lines could be present as a byproduct of the all-solid state reactions, carried out in the this investigation.

The stable compounds in the vicinity of the line CA-SA in Fig. 1 are: CA_2 (calcium di-aluminate or grossite), $C_{12}A_7$ (mayenite, C_2SA (di-calcium strontium aluminate), S_3A (tri-strontium aluminate), S_2A_3 (di-strontium tri-aluminate), S_4A_7 (tetra-strontium hepta-aluminate) and SA_2 (strontium di-aluminate), which has the similar structure as grossite (CA_2).

The nature and concentration of the crystallographic phases present in the ternary systems shown in Fig. 1 depend critically on factors such as firing temperatures, use of fluxes and firing
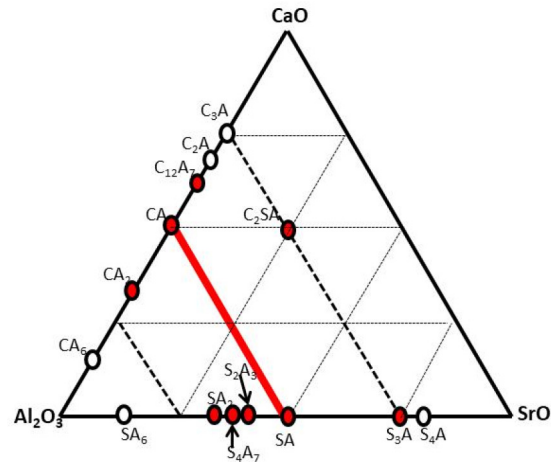
Fig. 1. Composition diagram of CaO-SrO-Al_2O_3. The cement chemistry notation has been adopted to denote the compounds in this ternary system. The red line indicates the compositions that were studied.

times, calcination procedures, etc.[13,14,29]. Furthermore, phases may change as a function of temperature as in the case of $SrAl_2O_4$ (monoclinic-hexagonal). Literature referring to phosphor performance in relation to preparation conditions has largely concentrated on the Sr-containing aluminates [30–32]. Cordoncillo et al. [31] reported that the hexagonal and monoclinic phases were confirmed in $SrAl_2O_4$:Eu^{2+}; after firing at 1000°C they obtained a hexagonal phase, which transformed into the monoclinic phase at lower temperatures, in agreement with the findings of Avdeev et al. [16]. Since the publications of Blasse and his co-authors [2,6] on $BaAl_2O_4$:Eu^{2+}, it is known that the measuring conditions, especially the temperature, have a substantial effect on the spectra. The influence of the processing conditions on the luminescence of $SrAl_2O_4$:Eu^{2+} nanoparticles that were produced by combustion methods were also reported [32].

As mentioned above, herein we shall focus on only a limited part of the ternary system of C-S-A, namely on the compounds formed on the line CA-SA ($Sr_{1-x}Ca_xAl_2O_4$, abbreviated CSA) in S-C-A. Ju et al. [33] recorded the CL spectra of CSA doped with Eu^{2+}. They measured a blue shift in going from x = 0 (pure Sr) to x = 0.1 and x = 0.3. The system CSA was also studied by Prodjosantoso and Kennedy [34] using X-ray diffraction; they found monoclinic CSA at the Ca-rich side and another monoclinic phase at the Sr-rich side. At 0.2 < x < 0.5 they also found a hexagonal phase based on the structure of $BaAl_2O_4$. Pöllmann and Kaden [35] also found 3 phases in CSA upon changing the ratio between Ca and Sr; their results confirmed largely the work of Prodjosantoso and Kennedy. Recently, the PL spectra of the system CSA doped with 5 mol% Eu^{2+} and 5 mol% Dy^{3+} have been published by Xie et al. [36]. The phases they found largely confirmed the results of Prodjosantoso and Kennedy and Pöllmann and Kaden.

In view of the scarcity of literature on the luminescent properties of CSA doped with only Eu^{2+} and the scientific debate over the origin of the two luminescence bands of $SrAl_2O_4$:Eu^{2+}, we decided to investigate the mixed aluminates doped with Eu^{2+} in more detail.

2.   Experimental

2.1.   Materials

Starting materials were: strontium carbonate (Sigma Aldrich, UK, 99.9%), calcium carbonate (Sigma Aldrich, UK, 99.9%), aluminum oxide (SASOL Inc., USA), europium oxide (Ampere Industrie, France, 99.99%), and concentrated hydrochloric acid (Sigma Aldrich, UK, 37%). All

materials were used as supplied without further purification. The final annealing of the powders was made in Al_2O_3 crucibles at high temperatures in H_2 (10%)/N_2 (90%) gas.

2.2. Synthesis

Solid state synthesis methods were used to prepare $Sr_{0.99-x}Eu_{0.01}Ca_xAl_2O_4$ with x varying between 0 and 0.99 in steps of 0.1. The samples were prepared by calcining mixtures of an appropriate molar ratio of $SrCO_3$, $CaCO_3$, γ-Al_2O_3 and $EuCl_3$ powders in a flow of 90% N_2–10% H_2. After calcination the powders were carefully ground by ball milling (Al_2O_3) for 3 hours. The final annealing of the $Sr_{0.99-x}Eu_{0.01}Ca_xAl_2O_4$ samples was at 1400°C under H_2/N_2 for 2 hours. In the wake of the work of Abbruscato [5] we also varied the molar ratio between SrO and Al_2O_3 in $SrAl_2O_4$ and found maximum PL at 5% excess Al_2O_3. For that reason it was decided to prepare all samples of $Sr_{0.99-x}Eu_{0.01}Ca_xAl_2O_4$ with 5% excess Al_2O_3 with respect to the sum of alkaline earth moles. The molar ratio x_{Ca} in this article refers to the molar ratio between Ca and Sr in the compounds.

2.3. Characterisation

The crystalline phases of the products were determined by X-ray powder diffraction at room temperature using Bruke's D8 Advance X-ray diffraction (XRD) equipment fitted with a nickel-filtered copper source, $CuK\alpha$ at λ=1.5406 Å, and a LynxEye silicon strip detector. Diffraction peaks were recorded at $5° < 2\theta < 100°$ and 25°C. The diffractometer was calibrated using an Al_2O_3 line position standard from Bruker and a LaB_6 NIST SRM 660a line profile standard. Diffractograms were collected using the fired powders in a conventional holder. The emission of the X-ray source and hence the instrumental line broadening was determined by fitting the NIST standard using Bruke's Topas (version 5) software package. Crystalline phases in the prepared samples were identified from the XRD-patterns by peak-search matching using the ICCD PDF-2 data files. The identifiable phases were refined according to the Rietveld procedures using the Topas package. The fundamental parameters approach was used. Fits were made taking into consideration the easily identified phases and taking into account how the phase ratios vary according to the observed data across the calcium / strontium range studied. Hence, phases were included in the Rietveld refinements even at low concentrations according to this procedure. R-Bragg values were fairly constant for each phase identified and R_{wp} values were in the range of 8 to 16.

Variable temperature X-ray powder diffraction measurements were performed on a Rigaku Oxford Diffraction (ROD), SuperNova, Dualflex, AtlasS2 X-ray diffractometer equipped with an Oxford Cryosystems Cobra plus variable temperature device. The X-ray source was a fine-focus, $CuK\alpha$, Enhance microsource, ($\lambda = 1.54184$ Å) and the detector an AtlasS2 CCD. A small amount of powder was distributed on the tip of a 50 μm MiTeGen mount and X-ray powder diffraction patterns were accumulated using the "Powder Power Tool" application from the CrysAlis PRO 1.171.39.44a operating software (Rigaku OD, 2015), which controls both the data collection and data reduction process. Data were accumulated using four θ settings for the detector, two positive and two negative, with different exposure times for the high and low angle segments and merged to give a final powder pattern. Data were collected at 290 K and 100 K for undoped $SrAl_2O_4$.

Morphology and particle size assessment of the phosphor powders were conducted in a scanning field emission electron microscope (FESEM), Supra 35 VP (Carl Zeiss, Germany). Some samples were also investigated in a transmission electron microscope (TEM), (2100F, JEOL, Japan) equipped with a Schottky-type field emission gun. The TEM was equipped with a Vulcan CL detector, Gatan, USA, for imaging and spectroscopic purposes. This system used a Czerny–Turner spectrometer with back-illuminated CCD and gratings with 1200 or 2400 grooves per mm for collection of CL emission spectra. A small cryostat connected to the sample holder

enabled cooling of the samples in the TEM down to 103 K (-170°C); adjustment of the sample temperature anywhere between 103 K and 303 K could be made.

PL excitation and emission spectra of the samples were recorded using a Bentham phosphor spectrometer system (Bentham Instruments Ltd., Reading, UK.), configured with M300 excitation and emission monochromators, which were equipped with 0.2 mm slits. The absolute wavelength calibration of this emission monochromator had maximal error of 0.4 nm; however, relative wavelength values were accurate within 0.05 nm.

3. Results

3.1. Electron microscope

The particle size of the alkaline earth aluminates after the high temperature annealing process was in all cases rather large and varied from about 1 to 6 μm. Figures 2a-2d are electron microscope images of samples after the final annealing step.

Figure 2(a) shows that crystallites sinter and form agglomerates. At temperatures >1400°C there is more sintering and the agglomerates grow in size. For this reason we have limited the annealing temperatures to 1400°C. Figs. 2(c) and 2(d) are STEM images of the particle shown in Fig. 2(b). Figure 2(d) is a panchromatic image; it indicates that the CL from phosphor particles depends on the thickness. At the edge the particle is rather thin and the CL is much weaker.
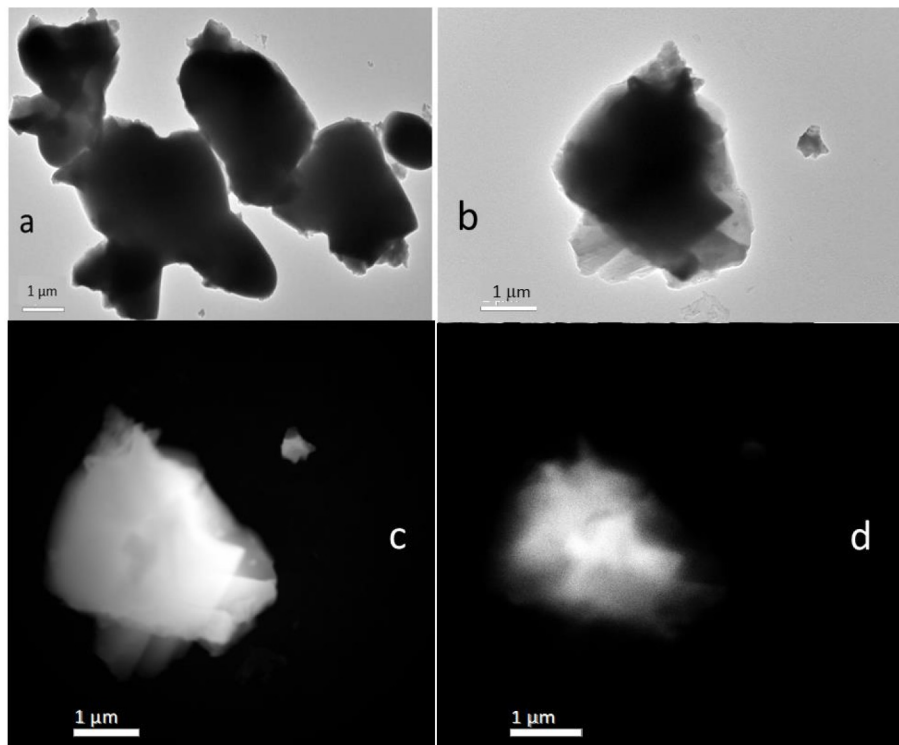
Fig. 2. (a) TEM image at 200 keV of $SrAl_2O_4$:1%Eu^{2+} annealed at 1400°C. (b) TEM image at 200 keV of $CaAl_2O_4$:1%Eu^{2+}. (c) STEM image (high-angle annular dark-field) of $CaAl_2O_4$:1%Eu^{2+}, same particle as in (b), slightly rotated. (d) Panchromatic image of the same particle (STEM).

3.2. X-ray diffraction and crystal structure

Figures 3(a) and 3(b) present powder XRD-diffractograms of $Sr_{0.99-x}Ca_xEu_{0.01}Al_2O_4$ $(0 \leq x \leq 0.99)$. By comparing the XRD-diffraction patterns of the $Sr_{0.99-x}Ca_xEu_{0.01}Al_2O_4$ series in Fig. 3(a) with powder diffraction files (PDF) of the compounds that are located in the vicinity of the SA-CA line in Fig. 1, we have identified five different phases in this phosphor series. These are listed in Table 1. Atomic coordinates and isotropic thermal parameters were not refined. Figure 11 in the appendix shows a typical example of the quality of the fit between the experimental a calculated XRD pattern for $Ca_{0.99}Eu_{0.01}Al_2O_4$. The difference between these two patterns is also indicated.
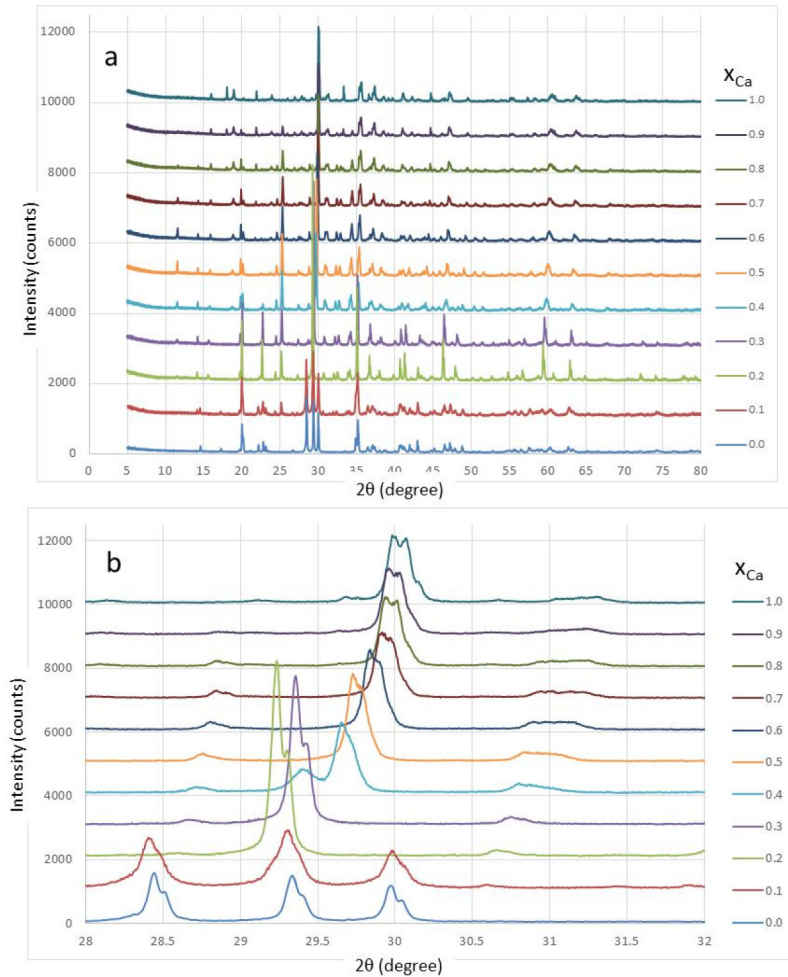
Fig. 3. Powder XRD-patterns of $Sr_{0.99-x}Ca_xEu_{0.01}Al_2O_4$ for $0 \leq x_{Ca} \leq 0.99$. (a) $10° \leq 2\theta \leq 80°$. (b) Enlarged pattern for the range $28° \leq 2\theta \leq 32°$. The diagrams for $0.02 \leq x_{Ca} < 0.1$ have not been indicated.

Cell parameters of compounds that are present in concentrations >10 mol % are listed in the appendix. Unlike monoclinic CA and monoclinic CA_2, which are present over a wide concentration range of Ca, the monoclinic SA and hexagonal phases can only exist at a limited Ca concentration range.

The compounds CA_2 (3) and $C_{12}A_7$ (5) are also known under the mineralogy names grossite and mayenite respectively. Cubic mayenite is present at high Ca content in small concentration

Table 1. Observed phases in $Sr_{0.99-x}Ca_xEu_{0.01}Al_2O_4$ phosphor series

Number	Compound	Crystal type	Space group	Table No. in appendix	Reference
1	SA	Monoclinic	$P2_1$	2	15,16,34,35
2	CA	Monoclinic	$P2_1/n$	3	17,34,35
3	CA_2	Monoclinic	C2/c	4	37–39
4	$C_{0.7}S_{0.3}A$	Hexagonal	$P6_3$	5	18–20,34,35
5	$C_{12}A_7$	Cubic	I43d	n.a.	40

only and is therefore not listed in the appendix. The cell constant found for this material agreed with the published value [38]. The comparison with literature data on the cell parameters in non-mixed alkaline earth aluminates is also indicated in the appendix tables (Tables 2–5). The phases 1 and 2 in Table 1, monoclinic $SrAl_2O_4$ and monoclinic $CaAl_2O_4$ respectively, are abbreviated as MCSr and MCCa in this work.

Figure 4(a) illustrates the compositions of the phases that we found in the CSA system, while Fig. 4(b) depicts the phases and compositions found by Prodjosantoso and Kennedy [34]. The eye-catching difference between Figs. 4(a) and 4(b) is the presence of large quantities of grossite, (CA_2+SA_2), in Fig. 4(a), whereas Prodjosantoso and Kennedy [34] and Pöllmann and Kade [35] did not find any grossite. As mentioned in section 2.2 we made our samples with 5% excess of Al_2O_3. We assumed that this was the main cause for the presence of grossite. This hypothesis was checked by repeating the synthesis of $Sr_{0.49}Eu_{0.01}Ca_{0.5}Al_2O_4$ without excess of Al_2O_3. In this case we did not find grossite either. From Fig. 4(a) it can be derived that the rather large quantity of Al_2O_3 stored in grossite at $x_{Ca}=0.49$ needs to be compensated by CaO + SrO in other phases to account for the mass balance. These phases were not present in crystalline form, but likely in the amorphous state. We tried to fit the back ground curve of the XRD-patterns at low 2θ-values to the quantity of amorphous material, but this procedure was unsuccessful. Nevertheless, it is assumed that CaO and SrO in amorphous state make up the mass balance.
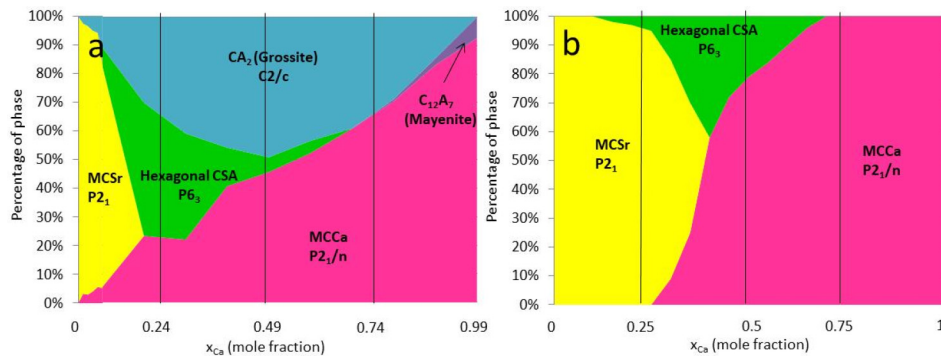
Fig. 4. Composition diagram of the phases in $Sr_{0.99-x}Ca_xEu_{0.01}Al_2O_4$ as determined from the XRD-measurements at room temperature. (a) This work. (b) Diagram based on the data published by Prodjosantoso and Kennedy [34].

MCSr has two sites for the alkaline earth cations, Sr(1) and Sr(2), which are located in two different channels formed by the AlO_4 tetrahedra along the c-axis [15,16]. Both cation sites have nine nearest neighbour O^{2-} ions, which belong to six different AlO_4 tetrahedra. Schulze and Müller-Buschbaum [15] commented on the curious distribution of the Sr-O distances for both Sr-sites: three of these distances are > 3 Å and cannot be considered to create a strong Sr-O bond. This conclusion is based on the radii of Eu^{2+}, Ca^{2+}, Sr^{2+}, Ba^{2+} and O^{2-} ions in six coordination arrangement, which are 1.31 Å, 1.14 Å, 1.32 Å, 1.49 Å and 1.26 respectively [41]. The other

six Sr-O bonds have an average distance of about 2.62 Å, which is only slightly more than the sum of the O^{2-} and Sr^{2+} radii. Schulze and Müller-Buschbaum [15] evaluated the effective coordination numbers (N), which are 6.07 and 6.23 for Sr(1) and Sr(2) respectively. Only Schulze and Müller-Buschbaum [15] published a list with all nine Sr-O bond distances for both the Sr(1) and the Sr(2) sites in $SrAl_2O_4$. When comparing their results with our data, we found a perfect match for the Sr-O bond distances of Sr(1), but for Sr(2)-O distances we observed a difference that is much larger than the error bar. We used PDF number 76-7488 in the refinements, which is based on the work of Avdeev et al. [16]. We found also differences between the average Sr(2)-O distance of Dutczak et al. [24] and Clabau et al. [25] and the average Sr(2)-O distance determined in this work, namely 2.72 Å for N = 9 and 2.60 Å for N = 7, whereas our result agrees with the average Sr(2)-O distance for N = 9 published by Botterman et al. [26]. The issue for this determination of the crystal structure is (1): the structures with two Sr^{2+} cation sites and 6 independent oxygen atom positions were calculated from a small number of XRD-patterns, and (2): most of the electron density is arising from the heavier Sr^{2+} cations, so the calculated positions of the oxygens show a rather large spread. After analysis of the various crystallographic information files (CIF) in the ICSD database for monoclinic $SrAl_2O_4$ ($P2_1$), we conclude that the refinement result depends on the choice for the CIF, which leads to slightly different atomic coordinates for the oxygen atoms: in other words, this choice causes the disagreement.

The next phase at $x_{Ca} \geq 0.2$ in Fig. 4(a) is the monoclinic phase of calcium di-aluminate: the grossite structure. This structure has one cation site, which is seven-coordinated. Although this structure has only one cation site, it is important considering where the Sr^{2+} is located, since the Eu^{2+}, responsible for PL, is closer in size to Sr^{2+} than to Ca^{2+}. Since the Eu^{2+} ion is slightly smaller in size than Sr^{2+}, it will predominantly occupy Sr^{2+}-sites and can only be forced into the smaller cation sites in the presence of an excess of Sr^{2+}. From the Rietveld refinements it was concluded that the Sr^{2+} cation occupancy in grossite is constant between x = 0.3 and 0.6, while the composition in the samples did not change significantly either. It is thus to be expected that this structure will not strongly affect the luminescence in this concentration range, apart from an effect on the band broadening. Figure 4(a) indicates that MCCa is the dominant phase in $Sr_{0.99-x}Ca_xEu_{0.01}Al_2O_4$. Its unit cell contains 12 $CaAl_2O_4$ formula units and has three alkaline earth cation sites, which are labelled Ca(1), Ca(2) and Ca(3), having equal multiplicity. The first two sites are six-coordinated, in which the O^{2-} anions belong to four different AlO_4 tetrahedra [17]. These cationic sites are located in one of the channels formed by the rings made by the AlO_4 tetrahedra. The cation site Ca(3) is different, since it is located in a second set of channels and it has nine O^{2-} anion nearest neighbours belonging to five different AlO_4 tetrahedra. Six of these nine O^{2-} anions are shared by two Ca(3) cations forming an elongated octahedron (thereby forming a continuous chain of the type Ca(3)-O-Ca(3)). The other three O^{2-} anions are in a plane perpendicular to this chain. We found that the Sr^{2+} cations in $Sr_{1-x}Ca_xAl_2O_4:Eu^{2+}$ prefer the Ca(3) sites at 0.4 < x < 0.9 and it is only around $x_{Ca} = 0.2$ that the three sites become equally populated with Sr^{2+}. Both MCCa and MCSr in $Sr_{0.99-x}Ca_x Eu_{0.01}Al_2O_4$ show a monotonous decrease of their cell volumes upon increasing x_{Ca}.

Figure 4(a) furthermore indicates that a hexagonal phase exists in the $Sr_{0.99-x}Ca_xEu_{0.01}Al_2O_4$ series at 0.1 < x < 0.6. Prodjosantoso and Kennedy [34] found that the hexagonal phase in $Sr_{1-x}Ca_xAl_2O_4$ was present at 0.35 < x < 0.65 with its maximum occurring at x = 0.4 as shown in Fig. 4(b). The hexagonal phase in $Sr_{0.99-x}Ca_xEu_{0.01}Al_2O_4$ is isostructural with $BaAl_2O_4$: both having space group $P6_3$. It should be realized that $BaAl_2O_4$ shows a phase transition from the paraelectric state (space group $P6_322$) at high temperature to the ferroelectric state (space group $P6_3$) by cooling down below ≈ 450 K [19,20]. At this phase transition the cell parameter "a" doubles from 5.22 Å to 10.44 Å [20] while the positions of the Ba and Al ions are slightly displaced [18,19]. In the case of hexagonal BA in the $Ba_{0.97-x}Sr_xEu_{0.03}Al_2O_4$ series we actually find that a = 10.4452 Å, while in the hexagonal phase of $Sr_{0.99-x}Ca_xEu_{0.01}Al_2O_4$ it is 10.1943 Å

at x_{Ca}=0.27, which is about 2% smaller, "apparently" reflecting the decrease of cation size in going from Ba^{2+} to Sr^{2+}. We use the adverb apparently as the change in cell parameter "a" size is in fact not as large as would be expected from the change in ionic radius from Sr^{2+} to Ba^{2+} and this must indicate that the network of connected AlO_4 tetrahedra is the dominating building block of the lattice and the cations are sitting in spaces that are not too constrictive. The assignment of very weak reflections in the XRD-pattern, from which the space group for the hexagonal phase of pure $BaAl_2O_4$ can be identified [18–20], is particularly difficult in the $Sr_{0.99-x}Ca_xEu_{0.01}Al_2O_4$ samples with contaminating compounds such as mayenite and grossite present.

3.3. PL and CL spectra

In Fig. 5 the PL spectra of the phosphor series $Sr_{0.99-x}Ca_xAl_2O_4$:1%Eu^{2+} have been plotted for various values of the molar fraction of one of the alkaline earth ions.
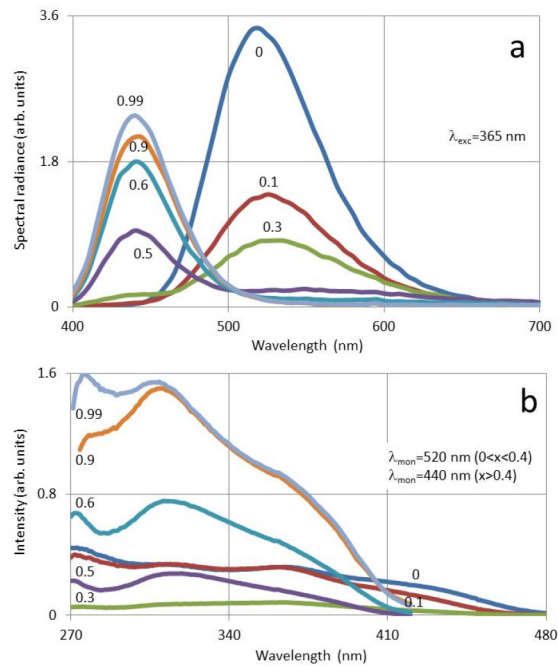
Fig. 5. Photoluminescence spectra of $Sr_{0.99-x}Ca_xAl_2O_4$:1%Eu^{2+} at various values of x_{Ca}. (a) Emission spectra. (b) Excitation spectra. For clarity reasons only a limited number of spectra are shown.

The PL spectra illustrated in Figs 5(a) and 5(b) agree nicely with the spectra published by Xie et al. [36]. A feature of the emission spectra in Fig. 5(a) is the asymmetric shape of the main emission band, viz. the band show a tail at the long wavelength side. This is even the case in a wavenumber representation of the spectra, which reduces the asymmetry slightly. This kind of asymmetry is usually observed in the fluorescence spectra of Eu^{2+} doped phosphors [1,24]. The standard explanation of this phenomenon is the presence of more than one site for the Eu^{2+} ion in the lattice: different sites create different electrostatic fields, so the presence of two or more sites would explain the asymmetry. However, the presence of more than one site for the Eu^{2+} does not explain that the tail is at the long wavelength side in the vast majority of Eu^{2+} doped phosphors. Another explanation of the asymmetry may be due to electron-phonon coupling, which can be described in terms of the Huang-Rhys parameter, the lattice vibrational energy and the line width of vibronic transitions [42]. From Figs. 5(a) and 5(b), using also the deconvolution

of the excitation spectrum presented in Fig. 10(a) hereafter, the Stokes shift for the 520 nm band of $SrAl_2O_4$:Eu^{2+} can be estimated as 4200 cm^{-1}, which is close to the estimate (4000 cm^{-1}) made by Poort et al. [6] and larger than the value (3500 cm^{-1}) reported by Botterman et al. [26]. The Huang-Rhys parameter S is calculated to be 5.1 (assuming an average lattice vibration of 450 cm^{-1}) for $SrAl_2O_4$:Eu^{2+}; then, according to the calculations presented by de Jong et al. [42], asymmetric broadening of a rare earth electronic transition will be unlikely. For this reason we decided to analyse the asymmetry of the fluorescence bands by deconvolution and to assign the profiles to Eu^{2+} ions positioned at alkaline earth sites in the lattice (whenever possible). This will be discussed in the next sections.

The emission spectra presented in Fig. 5(a) show that single alkaline earth aluminates have higher spectral radiances than aluminates with two alkaline earth ions. The spectra in Fig. 5(a) feature broadening of the emission band at mole fractions between 0.3 and 0.7. The spectra also indicate that the spectral radiance at x_{Ca}>0.47 is largely determined by the $CaAl_2O_4$ content in the samples. λ_0 in these spectra is close to 445 nm. Figure 5(a) manifests furthermore the large difference between the maximum spectral radiance at x_{Ca}=0 ($Sr_{0.99}Eu_{0.01}Al_2O_4$) and x_{Ca}=0.1 ($Sr_{0.89}Ca_{0.1}Eu_{0.01}Al_2O_4$). This substantial decrease in spectral radiance occurred largely between x_{Ca} is 0 and 0.04 and it indicates that the luminescence of monoclinic $SrAl_2O_4$ is very sensitive to relatively small changes of its structure as found by Abbruscato in 1971 [5]. As mentioned above, we have confirmed Abbruscatós result [5] by synthesizing $SrAl_2O_4$:Eu^{2+} phosphors with various SrO/Al_2O_3 molar ratios, close to unity, and investigating their PL spectra and XRD-patterns. We found that the spectral radiance at 515 nm increased by 40% by lowering the SrO/Al_2O_3 molar ratio to 0.95, while the structure remained essentially MCSr. The spectra presented in Fig. 5(a) also show the largest colour change: from green at the Sr-rich side to deep blue at the Ca-rich side; however, the rather low spectral radiance at $0.1 < x_{Ca} < 0.5$ makes this phosphor system not particularly attractive for colour tuning in display or lighting devices. We shall describe the analyses the PL and CL spectra of the system CSA in the next two sections. The first is focussing on $SrAl_2O_4$:Eu^{2+} and the MCSr phases with a small quantity of Ca, the second is focussing on $CaAl_2O_4$:Eu^{2+} and MCCa with a small amount of Sr.

3.3.1. $SrAl_2O_4$:Eu^{2+}

In Fig. 6 we present deconvolutions of PL-spectra of the MCSr phases of the $Sr_{0.99-x}Ca_xAl_2O_4$:1%Eu^{2+} series that are presented in Fig. 5(a), viz. the spectra at x_{Ca}=0 and 0.1. The fitting of the deconvoluted spectrum to the experimental spectrum was carried out using a least squares algorithm in a wavenumber (cm^{-1}) representation as described previously [43,44]. In the deconvolutions we have taken the minimum number of profiles that gave a good fit with the experimental spectra. The radiance R of a (Gaussian) profile is the area under the curve, often indicated in the literature as integrated intensity.

The PL spectrum of $SrAl_2O_4$:Eu^{2+} at room temperature as shown in Fig. 6(a) can be decomposed into two Gaussian profiles, p1 and p2. From the PL spectra of $SrAl_2O_4$:Eu^{2+},Dy^{3+} recorded between 100 K and 500 K by Ueda et al. [45], it can be concluded that their main emission band also consisted of two profiles. The wavelengths of p1 and p2 in Fig. 6(a) are 545 nm and 513 nm respectively; the radiance R of p1 is smaller: R_{p2}/R_{p1}=1.54. Ngaruiya et al. [28] published the deconvoluted PL spectrum of $SrAl_2O_4$:Eu^{2+},Dy^{3+}. They also found that the emission band can be described by two Gaussian profiles at λ_0 = 528 nm and 567 nm respectively, which deviates from our result presented in the table inserted in Fig. 6(a). This difference is likely caused by another excitation wavelength (325 nm) and their choice for a wavelength base in executing the deconvolution. When a small quantity of Ca is introduced in the MCSr phase, a third profile emerges at the high wavenumber side as shown in Fig. 6(b). The radiance of this peak increases when increasing the quantity of Ca, however, the radiance of the p3 profile is small compared to the radiances of the p1 and p2 profiles. Figure 7 illustrates the deconvolution of a CL spectrum

recorded at -169.5°C of $Sr_{0.99}Eu_{0.01}Al_2O_4$. The radiance (CL) of p3 is almost equal to the radiances measured by Clabau et al. [25] and Botterman et al. [26] at 100 K and excitation with UV radiation at 310 nm and 370 nm respectively.
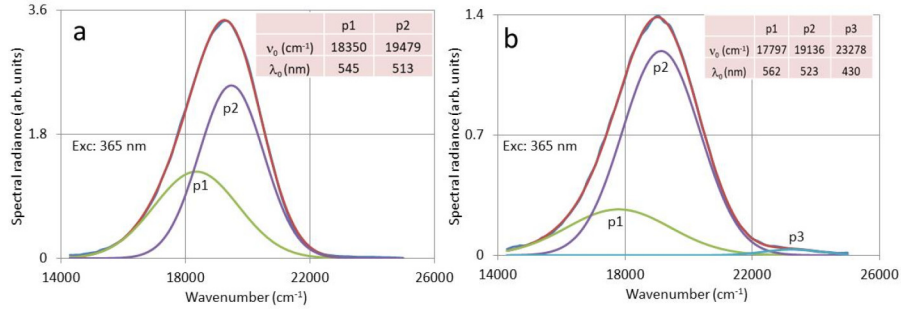
Fig. 6. Deconvolution of PL spectra of $Sr_{0.99}Eu_{0.01}Al_2O_4$ (a) and $Sr_{0.89}Ca_{0.1}Eu_{0.01}Al_2O_4$ (b) with 2 or 3 Gaussian profiles respectively. The inserts show the wavenumber and wavelength at the maximum spectral radiance of the profiles.
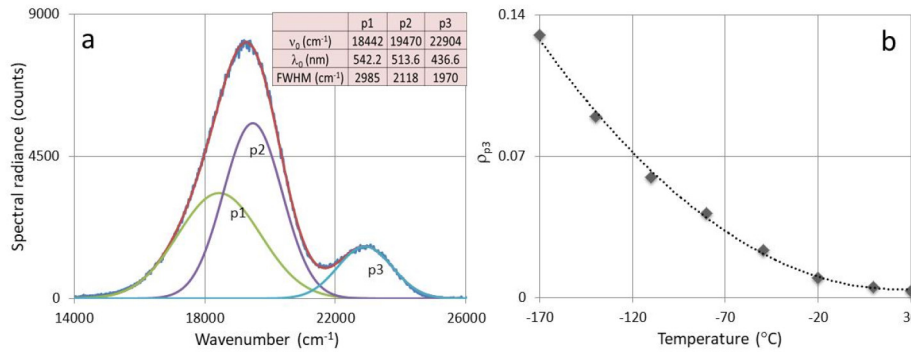
Fig. 7. (a) Deconvolution of CL spectrum of $Sr_{0.99}Eu_{0.01}Al_2O_4$ recorded at 200 keV and -169.5°C. The labelling of the profiles is equal to that in Fig. 6. (b) Normalized radiance of p3 versus temperature.

The normalized radiance of the p3 profile has been plotted versus temperature in Fig. 7(b): at room temperature this profile has virtually disappeared, which agrees with the data of Botterman et al. [26].

In Fig. 8 the normalised radiance of p3 has been plotted versus the mole fraction of Ca in $Sr_{0.99-x}Ca_xEu_{0.01}Al_2O_4$. The normalized radiance ρ_{pi} of profile pi is:

$$\rho_{pi} = \frac{R_{pi}}{R_{p1} + R_{p2} + R_{p3}} \tag{1}$$

Figure 8 provides the evidence that the p3 profile can be assigned to the emission of the MCCa phase with space group P2$_1$/n. This assignment is obvious at $x_{Ca}>0.5$, where the concentration of the MCCa phase is increasing, while the concentration of CA$_2$ (grossite) is strongly decreasing (compare Fig. 4(a)). At $x_{Ca}<0.2$ the radiance of p3 and the concentration of MCCa behave identically. Although the grossite phase (CA$_2$) also increases at $0 < x_{Ca}<0.2$, we may exclude this latter phase as a candidate for the p3 profile because of the behaviour of ρ_{p3} at $x_{Ca}>0.5$.

Clabau et al. [25] and Ngaruiya et al. [28] assigned the two bands p1 and p2 in Figs. 6 and 7 to Eu^{2+} ions that are positioned at the Sr(1) and Sr(2) cation sites in monoclinic SrAl$_2$O$_4$.
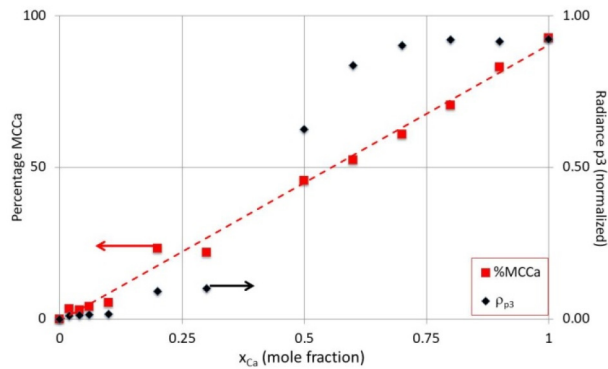
Fig. 8. Percentage of MCCa and normalised radiance of p3 versus x_{Ca}. The straight line and the curves have been fitted to the data points to guide the eye.

According to Poort et al. [6], Botterman et al. [26] and Dutczak et al. [24] this is not the case: p3 and the combination p1-p2 should be assigned to Eu^{2+} at Sr(2) and Sr(1) respectively. The work of Botterman et al. presents an extensive study of the PL from $SrAl_2O_4:Eu^{2+}$ and supports this conclusion. The conclusion has recently been confirmed in a theoretical study by Ning et al. [45]. They found that the p3 profile of $SrAl_2O_4:Eu^{2+}$ at 440 nm is due to the 5d-4f emission of Eu^{2+} situated at the Sr(2) site. Unfortunately, these recent studies do no address Clabaús point [25]: by combining p1 and p2 profiles to one emission band, the band gets asymmetric. This asymmetry was not considered in the studies mentioned above. Ueda et al. [46] and Nazarov et al. [47] explained the disappearance of p3 at high temperature by energy transfer (down conversion) from the Eu^{2+} at the Sr(1) to Eu^{2+} at Sr(2). These Eu^{2+} ions differ in preferential orientation of the 5d orbitals of Eu^{2+} at Sr(1) and Sr(2). Nevertheless, we agree with the conclusion of Nazarov et al. that there is still no satisfactory explanation in the literature to account for the origin of the p3 profile.

Based on the similarity of the PL and CL measurements presented in Figs. 6(b) and 7(b) respectively, here we would like to discuss an alternative mechanism, namely a phase transition of the MCSr structure to MCCa at low temperature. The three alkaline earth sites in MCCa, viz. Ca(1), Ca(2) and Ca(3), when occupied by Eu^{2+} ions, explain the occurrence of p1, p2 and p3 at low temperature in $SrAl_2O_4:Eu^{2+}$ and at small Ca^{2+} mole fractions in $Sr_{1-x}Ca_xAl_2O_4:Eu^{2+}$. Hence, what occurs in $SrAl_2O_4$ at high temperature, a transition from the monoclinic to the hexagonal phase, takes place in reversed sense at low temperature: transition from the MCSr phase (space group $P2_1$) to the slightly more distorted MCCa phase (space group $P2_1/n$) with three cation sites. This phase transition does not occur at one temperature but takes place gradually: upon lowering the temperature the MCCa quantity will increase, which explains the increase of the p3 signal at about 440 nm, being the emission maximum of $CaAl_2O_4:Eu^{2+}$ (Fig. 5(a)). As mentioned above, XRD-data on $SrAl_2O_4$ at cryogenic temperatures have not been found in the literature. Nevertheless, we found support for the alternative hypothesis presented above by comparing the excitation spectra of $CaAl_2O_4:Eu^{2+},Dy^{3+}$ and $SrAl_2O_4:Eu^{2+},Dy^{3+}$ at cryogenic temperatures by Ueda et al. [48] and Botterman et al. [26] respectively. The excitation spectrum of the latter compound, when monitored at λ_0 of the p3 profile (440 nm), is almost similar to the excitation spectrum of $CaAl_2O_4:Eu^{2+},Dy^{3+}$ monitored at 440 nm. A second consideration refers to the measurement of the decay time of the green and blue bands of $SrAl_2O_4:Eu$ published by Botterman et al. [26]. These authors found that the decay curve of the green emission band can be described with two exponentials. This does not contradict with the alternative presented here: their result could also be explained in terms of a double emission centre with Eu^{2+} ions at the Sr(1) and Sr(2) sites. Botterman et al. [26] and Bierwagen et al. [49] determined the

1/e-value of the decay curve of the blue band at 0.1-0.2 μs at room temperature, which is (almost) equal to the decay constant of the emission band of $CaAl_2O_4:Eu^{2+}$ [1]. Finally, Bierwagen et al. presented an energy transfer model from Eu^{2+} positioned at Sr(2) (blue emission) to Eu^{2+} at the Sr(1) site (green emission). This model does not easily comply with our alternative hypothesis; however, on the other hand it is not obvious either to explain the increase of the p3 profile by doping $SrAl_2O_4$:Eu with a small quantity of Ca in terms of an energy transfer model. It is worth commenting on the fact that the increase of the p3 profile by doping $SrAl_2O_4$:Eu with a small quantity of Ca as reported herein is contrary to what would have been expected by an energy transfer model. Such a model predicts better energy transfer if the lattice decreased in size as the Eu^{2+} cations would be closer together, which is the case here, so it would not be expected that the p3 band would be observed at room temperature. The fact that the p3 profile is seen (Fig. 6(b)) we take as evidence that a smaller lattice stabilizes the small proportion of the low temperature phase (MCCa phase) so that it does not completely convert back at higher temperature. This explanation would be in keeping with the fact that the phase at room temperature switches over to the MCCa phase at just a little higher Ca concentration. The results on the 440 nm luminescence

A second issue is the discrepancy between the alternative hypothesis, presented above, and the assignment of the 440 nm band to Eu^{2+} at Sr(2) by Ning et al. [45] based on a multi-configurational ab initio study. It would be interesting to extend these calculations to Eu^{2+} positioned at the three alkaline earth sites in the $P2_1/n$ lattice ($CaAl_2O4$ lattice) for $SrAl_2O_4$. Although the alternative hypothesis put forward here cannot (elegantly) explain the results of Bierwagen et al. [49], we suggest that XRD-analyses of $SrAl_2O_4$ at low temperatures should be done to resolve the issues discussed above.

It is clear that the hypothesis about the nature of the low temperature p3 band in $SrAl_2O_4$ presented above can easily be tested by XRD at low temperature. We have recorded XRD-spectra of undoped $SrAl_2O_4$ annealed at 1350°C in H_2/N_2 at 100 K and 290 K. The result was that there was hardly any difference between these patterns and the conclusion must be that the hypothesis regarding $SrAl_2O_4$ without Ca has been shown to be false. This conclusion does not affect the result presented in Fig. 8, which presents a fair correspondence between the MCCa content and the radiance of the p3 profile in the $Sr_{0.99-x}Ca_xEu_{0.01}Al_2O_4$ compounds. In other words, although the similarity between the p3 profiles in Figs. 6(b) and 7(a) is striking, the nature of the two bands at 440 nm is different.

In a recent article about the luminescence of undoped $SrAl_2O_4$ Vitola et al. [50] attribute the 440 nm low temperature band to an F-centre as present in α-Al_2O_3. We believe that this is a more reasonable explanation and that as the temperature increases the energy in the F-centres transfers to the Eu^{2+} cations, where it is emitted as part of the emission bands. We will present this in more detail in another paper. We have previously studied energy transfer from intrinsic emission bands in Y_2O_3 caused by cathodoluminescence to Eu^{3+} cations depending on the concentration of the rare earth cation and believe a similar phenomenon is taking place here [51,52]. From this previous work it is perfectly reasonable to see emission from two different phenomena in the same material depending on temperature. In fact, the quantitative analysis of Bierwagen et al. [49] on the energy transfer in $SrAl_2O_4:Eu^{2+}$ is equally valid for the transference of energy from an F-centre (at 440 nm) to the Eu^{2+} cations (at 520 nm). Moreover we note that the lack of an isosbestic point in the temperature dependence of the spectra in the paper of Bierwagen et al. [49] is evidence that more than two species are present and this would fit with our interpretation of an F centre and two Eu^{2+} cation sites. An analysis of the occurrence of isosbestic points in the emission spectra of solids was published by Greger et al. [53]. We note that the absence of an isosbestic point was not addressed [49]. An examination of the data in Table 1 in the Bierwagen et al. [49] paper shows that the lifetime of the blue band decreases as the Eu^{2+} concentration increases; a fact that was not commented on either in the paper of Bierwagen et al. This is exactly what would be expected if energy were transferring from an F-centre to Eu^{2+} cations.

The F-centre itself would have a slow decay [54], but as the energy is transferred the decay would be measured faster and would depend on the number of Eu^{2+} cations present to which the energy could be transferred.

Further evidence for our assignment of the optical emission arises by considering the implications of the paper written by Denault et al. [55] for our results. A reviewer kindly suggested we should consider this paper. This paper considers "Average and Local Structure, Debye Temperature, and Structural Rigidity in Some Oxide Compounds Related to Phosphor Hosts"; one of the structures they studied was $SrAl_2O_4$. They refer to average Sr-0 bond lengths for Sr(1) of 2.680 Å assuming the site is 7 co-ordinate and for Sr(2) the average is 2.749 Å assuming this site is 8 co-ordinate. These values are larger than those we discussed in section 3.2 of this paper but are based on different coordination numbers and so are in reasonable agreement with our earlier discussion. More significantly Denault et al. analysed the Debye temperature of the lattice from a number of different methods and considered it relative to both local structure and longer range structure. They found that $SrAl_2O_4$ has a high Debye temperature and commented that the higher the value the more rigid the lattice. This is in keeping with the fact that this structure has all its AlO_4 tetrahedra fully three-dimensionally connected by the oxygen atoms. The authors stated that the higher degree of connectivity in $SrAl_2O_4$ leads to the higher Debye temperature observed. The results of this study provide evidence that the two Sr sites in the $SrAl_2O_4$ would not be expected to have very different thermal behaviour, and thus do not lend support to suggestions that the thermal dependence of emission from these two sites should be very different. In other words, the substantial differences between the behaviour of the 440 nm band and the main band at 520 nm in $SrAl_2O_4$ might be explained in terms of originating from different independent mechanisms for these bands.

3.3.2. $CaAl_2O_4$:Eu^{2+}

In Fig. 9 we present deconvolutions of PL and CL spectra of $CaAl_2O_4$:Eu^{2+} and two samples of $Sr_{1-x}Ca_xAl_2O_4$:Eu^{2+}.

The main emission band shown in Figs. 9(a), 9(b) and 9(d) is asymmetric and cannot be represented by a single Gaussian profile. Two Gaussian profiles can be fitted rather well to the main emission bands: these have about equal radiance and are close $(0.1 \pm 0.02\,eV)$ to each other. However, the main band of $Sr_{0.49}Ca_{0.5}Al_2O_4$:$Eu_{0.01}$ in Fig. 9(c) can be well described by a single Gaussian profile. This latter sample consists predominantly of two phases, grossite and MCCa as indicated in Fig. 4(a): this could be one of the reasons that the asymmetry in the MCCa band has disappeared. The other reason, which seems more likely, is that the occupancy of Sr for the Ca(3) site at this mole fraction of Ca is much larger than the occupancies for the other two sites. Since Eu^{2+} has about the same ion size as Sr^{2+}, we assume that this symmetric emission band indicates the emission from Eu^{2+} ions situated at Ca(3) in MCCa. The spectra illustrated in Figs. 9(a) and 9(b), which refer to $CaAl_2O_4$:Eu^{2+} without Sr, have been fitted with three Gaussian profiles respectively. In analysing the CL spectrum at -169°C of Fig. 9(b), we could not accurately determine the profile of q1: the insert of Fig. 9(b) indicates that there must be an emission signal at about 18500 cm^{-1}. The profile q0 in the CL spectra gradually disappeared upon increasing the temperature to 25°C. The q2 and q3 profiles are assigned to the Eu^{2+} ions at the Ca(3) site in $CaAl_2O_4$. As discussed in section 3.2, the Ca(3) site in the $P2_1/n$ lattice of $CaAl_2O_4$ is roomy and can easily lodge the Eu^{2+} ion. From the asymmetry of the 440 nm band it must be concluded that there are two positions for the Eu^{2+} ions at the Ca(3) lattice site. As the radiances of q2 and q3 are almost equal, it is likely that these two Ca(3) sites have equal probabilities of being occupied. This conclusion includes that $CaAl_2O_4$ would be ferroelectric as in the case of $BaAl_2O_4$.

The q1 profile is attributed to Eu^{2+} situated at the Ca(2) and Ca(1) sites, while q0 is assigned to europium trapped exciton (ETE) emission [46], which explains that this emission band
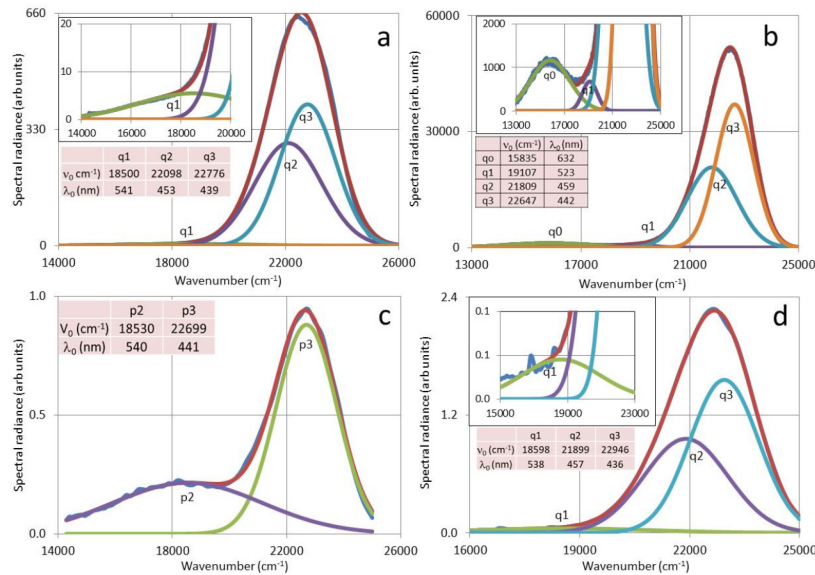
Fig. 9. Deconvolutions of PL and CL spectra of $CaAl_2O_4$:Eu^{2+} and CSA with three (or two) Gaussian profiles. The inserts show the profiles q0 and q1 at an enlarged scale. (a) PL spectrum of $Ca_{0.97}Al_2O_4$:$Eu_{0.03}$, exc. 340 nm. (b) CL spectrum $Ca_{0.97}Al_2O_4$:$Eu_{0.03}$, recorded at -169°C and 200 keV. (c) PL spectrum of $Sr_{0.49}Ca_{0.5}Al_2O_4$:$Eu_{0.01}$, exc. 365 nm. (d) PL spectrum of $Sr_{0.19}Ca_{0.8}Al_2O_4$:$Eu_{0.01}$, exc. 365 nm.

disappears at room temperature. Ueda et al. [48] studied the PL from $CaAl_2O_4$:Eu^{2+} at various temperatures and found the profiles q0 and q1 at 650 nm and 540 nm respectively. These values are somewhat larger than our results. A second difference is that their measurements indicated that the luminescence of q1 (540 nm) at room temperature is virtually zero. They also assigned the main emission at 440 nm to Eu^{2+} ions on the Ca(3) sites, but they did not consider the asymmetry of this emission peak. In contrast to the assignment of the 540 nm band by Ueda et al. [48] (who assigned it solely to Ca(2)); here it is assigned to both the Ca(1) and Ca(2) sites as they are both six-coordinated and only a very small amount of Eu^{2+} ions occupy these lattice sites. Finally it should be pointed out that the ETE emission does not need to be connected to one particular Eu^{2+} ion, but may rather be generated at the various sites, where Eu^{2+} ions are sitting, again in contrast to the suggestion of Ueda et al. [48].

3.4. Excitation spectra

We shall now briefly describe an analysis of the excitation spectra shown in Fig. 5(b) of the $Sr_{0.99-x}Ca_xEu_{0.01}Al_2O_4$ series: Fig. 10 manifests deconvolutions for a selection of excitation spectra of this system. These deconvolutions are necessary to obtain accurate values for the Stokes shift of electronic transitions, as described in the beginning of section 3.3. Nazarov et al. [47] have assigned the p4 profile in Fig. 10(a) to a charge transfer transition. Since this band persists in Figs. 10(b), 10(c) and 10(d), we assign p4 in these figures also to charge transfer. Figs. 10 show that the largest changes in the spectra occur between 10(a), 10(b) and 10(c). These changes refer largely to the p1 and p2 bands, while the p3 and p4 bands show only moderate changes. The disappearance of p1 in Fig. 10(c) may be caused by changing the monitoring wavelength from 520 nm to 440 nm, because in the excitation spectrum at x_{Ca}=0.3 monitored at 520 nm the p1 band is still present (not shown). According to Fig. 4(a) we have only monoclinic $SrAl_2O_4$:Eu^{2+} at x_{Ca}=0, and at x_{Ca}=0.2 and x_{Ca}=0.4 we have three phases: grossite, hexagonal

$Sr_{0.99-x}Ca_xAl_2O_4:Eu^{2+}$ and MCCa. We assume that p1 in Fig. 10(a) is attributed to the 4f→5d transition of Eu^{2+} in monoclinic $SrAl_2O_4:Eu^{2+}$, whereas in Fig. 10(b) it is attributed to the 4f→5d transition of Eu^{2+} in the hexagonal phase.
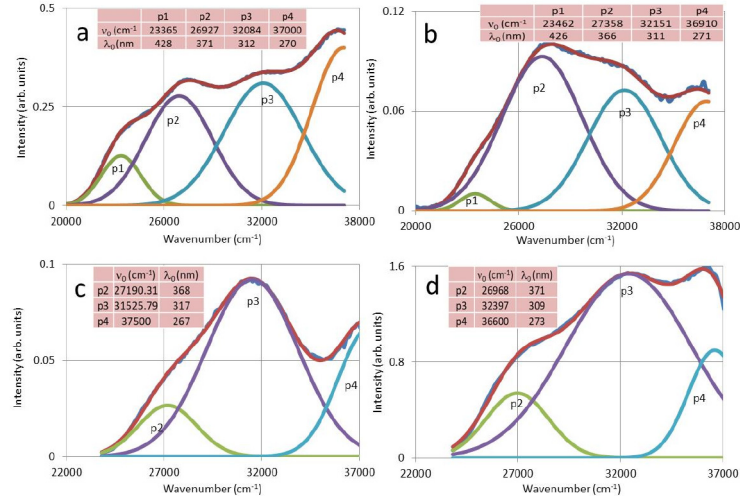
Fig. 10. Deconvolution of excitation spectra of $Sr_{0.99-x}Ca_xAl_2O_4:1\%Eu^{2+}$ with three or four Gaussian profiles. (a) $Sr_{0.99}Eu_{0.01}Al_2O_4$. (b) $Sr_{0.79}Ca_{0.2}Eu_{0.01}Al_2O_4$. (c) $Sr_{0.59}Ca_{0.4}Eu_{0.01}Al_2O_4$. (d) $Ca_{0.99}Eu_{0.01}Al_2O_4$. Note the difference of the abscissae between (a) and (b) on the one hand, and (c) and (d) on the other hand.

This assumption is also based on the fact that monoclinic $SrAl_2O_4$ transfers to the hexagonal phase at 670°C [16]. In Fig. 10(d) the p2 and p3 profiles are assigned to the 4f→5d transition of Eu^{2+} in MCCa; this assignment refers also to Fig. 10(c) because the monitoring wavelength for this spectrum is at 440 nm, the emission maximum of $CaAl_2O_4:Eu^{2+}$. Possible contributions from grossite and hexagonal $Sr_{0.99-x}Ca_xAl_2O_4:Eu^{2+}$ are likely too small to be distinguished in the spectrum of Fig. 10(c). The profiles p2 and p3 in Fig. 10(b) are attributed to the grossite and hexagonal phases in $Sr_{0.99-x}Ca_xAl_2O_4:Eu^{2+}$. Because of the complex character of excitation spectra due to the overlap between CT-bands and 4f-5d transitions, the above consideration is necessarily tentative.

4. Conclusions

Studies on the phases present and their luminescence in the solid state syntheses of the aluminate series CSA doped with Eu^{2+} yielded some expected and unexpected results. In the category of expected results we found and assigned a large number of phases, whereas amongst the unexpected was the finding of a large quantity of grossite. As discussed above, it is assumed herein that the rather large concentration of grossite found in the CSA samples is caused by the presence of the 5% excess of Al_2O_3 with respect to SrO + CaO. Evidence for this arises from the fact that when we did not use excess Al_2O_3 we did not find the presence of grossite.

The analyses of the PL spectra were largely based on deconvolutions of the emission bands. From the results reported here it can be concluded that this analysis technique is rather powerful. All deconvolutions of the spectra have been executed using a wavenumber base, because line broadening mechanisms are largely energy-related. Many deconvolutions of Eu^{2+} emission bands published in the literature are based on wavelength, which yield deviating parameters, particularly for ν_0 and FWHM, for profiles with FWHM > 1000 cm^{-1} (>0.12 eV) in the visible

range. Hence, in citing and comparing data on deconvoluted spectra from the literature, attention must be paid to the deconvolution algorithm.

From the analyses of the spectra of $SrAl_2O_4:Eu^{2+}$ at low temperature and with small Ca additions, herein we have discussed an alternative mechanism for the origin of the 440 nm emission band observed in $SrAl_2O_4:Eu^{2+}$ at low temperatures, namely that it is due to a phase transition that goes from monoclinic $SrAl_2O_4:Eu^{2+}$ with space group $P2_1$ to monoclinic $SrAl_2O_4:Eu^{2+}$ with space group $P2_1/n$, which is the space group of $CaAl_2O_4$. This phase transition was assumed to take place in $SrAl_2O_4:Eu^{2+}$ upon lowering the temperature. From XRD-measurements of $SrAl_2O_4$ at low temperature it was concluded that this alternative mechanism cannot be true: apart from the explanations in the literature, which do not account for the asymmetry of the 515 nm band of $SrAl_2O_4$, we believe that the assignment of the low temperature 440 nm band to an alumina F-centre is the most viable explanation. We intend to investigate this latter hypothesis in more detail and report this work in a future paper.

We also propose herein a new assignment of the bands in the spectrum of $CaAl_2O_4:Eu^{2+}$ based on the asymmetry of the main emission band that was ignored by previous researchers. From this latter asymmetry it also concluded that $CaAl_2O_4$ is ferroelectric, which has not been tested in this work any further.

Appendix
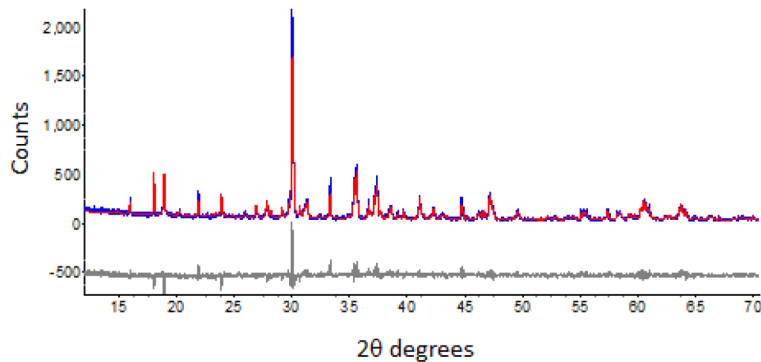
Fig. 11. Topas V5 refinements for $CaAl_2O_4:Eu$ 1%. The blue line is the experimental data, red is the calculated profile and the grey the difference profile.

Table 2. Monoclinic SA in $Sr_{0.99-x}Ca_xEu_{0.01}Al_2O_4$

Ca content (mole fraction)	Composition (%)	Unit cell parameters				
		a (Å)	b(Å)	c (Å)	β (°)	V(Å³)
0 *)	100.	8.447	8.816	5.163	93.420	383.8
0**)	100	8.444	8.822	5.160	93.411	383.7
0	100	8.442	8.821	5.159	93.410	383.5
0.02	94.3	8.440	8.825	5.154	93.405	383.2
0.04	93.6	8.434	8.822	5.151	93.425	382.6
0.06	90.6	8.429	8.819	5.149	93.441	382.0
0.08	88.6	8.424	8.818	5.148	93.468	381.7
0.1	78.1	8.420	8.816	5.146	93.487	381.3
0.2	0	n. a	n. a	n. a	n. a	n. a

*) Pure $SrAl_2O_4$ according to [15].
**) Eu^{2+} mole fraction = 0

Table 3. Monoclinic CA in $Sr_{0.99-x}Ca_xEu_{0.01}Al_2O_4$

Ca content (mole fraction)	Composition (%)	Unit cell parameters				
		a (Å)	b(Å)	c (Å)	β (°)	V(Å³)
0	0	n. a.	n. a.	n. a.	n. a.	n. a.
0.02	3.3	8.861	8.379	15.378	90.060	1141.6
0.04	3	8.860	8.368	15.373	90.048	1139.7
0.06	4.1	8.855	8.367	15.369	90.043	1138.7
0.08	5.8	8.860	8.401	15.357	89.990	1143.1
0.1	4.9	8.863	8.413	15.350	89.948	1144.5
0.2	23.3	8.847	8.396	15.329	89.893	1138.7
0.3	22	8.825	8.342	15.301	89.967	1126.3
0.4	40.7	8.786	8.214	15.282	89.907	1102.9
0.5	45.6	8.760	8.181	15.261	89.956	1093.7
0.6	52.3	8.741	8.144	15.232	89.946	1084.3
0.7	60.9	8.724	8.110	15.211	90.093	1076.2
0.8	70.5	8.715	8.105	15.205	90.106	1074.0
0.9	83.1	8.710	8.099	15.202	90.117	1072.3
0.99	92.6	8.704	8.096	15.203	90.128	1071.3
1.00*)	100	8.700	8.092	15.190	90.280	1069.4

*) Pure $CaAl_2O_4$ according to [17].

Table 4. Monoclinic CA$_2$ (Grossite) in Sr$_{0.99-x}$Ca$_x$Eu$_{0.01}$Al$_2$O$_4$

Ca content (mole fraction)	Composition (%)	Unit cell parameters				
		a (Å)	b (Å)	c (Å)	β (°)	V (Å^3)
0	0	n.a.	n.a.	n.a.	n.a.	n.a.
0.02	2.5	13.018	9.027	5.551	106.290	626.1
0.04	3.4	13.040	9.011	5.537	106.243	624.7
0.06	5	13.031	9.007	5.535	106.310	623.5
0.08	5.7	13.026	9.004	5.533	106.348	622.8
0.1	10.7	13.020	8.998	5.529	106.374	621.4
0.2	30	12.990	8.970	5.507	106.557	615.1
0.3	40.8	12.963	8.945	5.489	106.688	609.7
0.4	45.8	12.948	8.932	5.480	106.762	606.8
0.5	49.1	12.932	8.917	5.468	106.855	603.4
0.6	43.4	12.915	8.903	5.456	106.928	600.2
0.7	39.1	12.894	8.890	5.448	106.910	597.5
0.8	28.8	12.897	8.891	5.447	106.934	597.5
0.9	14.5	12.901	8.891	5.444	107.003	597.1
0.99	0	n. a.	n. a.	n. a.	n. a.	n. a.
1.00*)	100	12.84	8.862	5.431	106.830	591.5

*) Pure CaAl$_4$O$_7$ according to [34].

Table 5. Hexagonal (P6$_3$) CSA in Sr$_{0.99-x}$Ca$_x$Eu$_{0.01}$Al$_2$O$_4$

Ca content (mole fraction)	Composition (%)	Unit cell parameters		
		a (Å)	c (Å)	V (Å^3)
0.1	6.3	10.231	8.395	761.0
0.2	46.7	10.218	8.388	758.4
0.3	37.2	10.194	8.351	751.5
0.4	13.5	10.189	8.338	749.6
0.5	5.2	10.146	8.181	729.4
0.6	4.3	10.125	8.146	723.2

References

1. W. M. Yen and M. J. Weber, *Inorganic Phosphors* (CRC Press, 2004).
2. G. Blasse and A. Bril, "Fluorescence of Eu^{2+}-activated alkaline-earth aluminates," Philips Res. Rep. **23**, 201–206 (1968).
3. G. Blasse, W. I. Wanmaker, and J. W. Ter Vrugt, "Some new classes of efficient Eu^{2+}-activated phosphors," J. Electrochem. Soc. **115**(6), 673 (1968).
4. F. C. Palilla, A. K. Levine, and M. R. Tomkus, "Fluorescent properties of alkaline earth aluminates of the type MAl$_2$O$_4$ activated by divalent europium," J. Electrochem. Soc. **115**(6), 642–644 (1968).
5. V. Abbruscato, "Optical and Electrical Properties of SrAl$_2$O$_4$:Eu^{2+}," J. Electrochem. Soc. **118**(6), 930–933 (1971).
6. S. H. M. Poort, W. P. Blokpoel, and G. Blasse, "Luminescence of Eu^{2+} in barium and strontium aluminate and gallate," Chem. Mater. **7**(8), 1547–1551 (1995).

7. B. M. Mothudi, O. M. Ntwaeaborwa, J. R. Botha, and H. C. Swart, "Photoluminescence and phosphorescence properties of MAl_2O_4:Eu^{2+}, Dy^{3+} (M = Ca,Ba,Sr) phosphors prepared at an initiating combustion temperature of 500°C," Phys. B **404**(22), 4440–4444 (2009).

8. T. Matsuzawa, Y. Aoki, N. Takeuchi, and Y. Murayama, "A new long phosphorescent phosphor with high brightness, $SrAl_2O_4$:Eu^{2+},Dy^{3+}," J. Electrochem. Soc. **143**(8), 2670–2673 (1996).

9. K. Van den Eeckhout, P. F. Smet, and D. Poelman, "Persistent luminescence in Eu^{2+} -doped compounds: A Review," Materials **3**(4), 2536–2566 (2010).

10. J. Kaur, B. Jaykumar, V. Dubey, R. Shrivastava, and N.S. Suryanarayana, "Optical properties of rare earth-doped barium aluminate synthesized by different methods-A Review," Res. Chem. Intermed. **41**(4), 2317–2343 (2015).

11. Y. Lin, Z. Tang, Z. Zhang, and C. Nan, "Influence of co-doping different rare earth ions on the luminescence of $CaAl_2O_4$-based phosphors," J. Eur. Ceram. Soc. **23**(1), 175–178 (2003).

12. D. S. Kshatri and A. Khare, "Characterization and optical properties of Dy^{3+} doped nanocrystalline$SrAl_2O_4$:Eu^{2+} phosphor," J. Alloys Compd. **588**, 488–495 (2014).

13. P. Ptáček, *Strontium Aluminate - Cement Fundamentals, Manufacturing, Hydration, Setting Behaviour and Application* (InTech, 2014), Chap. 1.

14. R. C. Ropp, *Encyclopedia of the Alkaline Earth Compounds* (Elsevier, 2013), Chap. 6.

15. A.-R. Schulze and H. Müller-Buschbaum, "Compound Formation MeO:M_2O_3. IV. Structure of Monoclinic $SrAl_2O_4$," Z. Anorg. Allg. Chem. **475**(4), 205–210 (1981).

16. M. Avdeev, S. Yakovlev, A.A. Yaremchenko, and V.V. Kharton, "Transitions between $P2_1$, $P6_3(\sqrt{3}A)$, and $P6_32$ modifications of $SrAl_2O_4$ by in situ high-temperature X-ray and neutron diffraction," J. Solid State Chem. **180**(12), 3535–3544 (2007).

17. W. Hörkner and H. Müller-Buschbaum, "About the crystal structure of $CaAl_2O_4$," J. Inorg. Nucl. Chem. **38**(5), 983–984 (1976).

18. W. Hörkner and H. Müller-Buschbaum, "About the crystal structure of $BaAl_2O_4$," Z. Anorg. Allg. Chem. **451**(1), 40–44 (1979).

19. S. Y. Huang, R. Von Der Muehll, J. Ravez, and M. Couzi, "Phase transition and symmetry in $BaAl_2O_4$," Ferroelectrics **159**(1), 127–132 (1994).

20. A. M. Abakumov, O. I. Lebedev, L. Nistor, G. Van Tendeloo, and S. Amelinkx, "The ferroelectric phase transition in tridymite type $BaAL_2O_4$ studied by electron microscopy," Phase Transitions **71**(2), 143–160 (2000).

21. T. Aitasalo, J. Hölsa, H. Junger, M. Lastusaari, and J. Niittykoski, "Comparison of sol-gel and solid-state prepared Eu^{2+} doped calcium aluminates," Mater. Sci. **20**(1), 15–20 (2002).

22. B. Smets, J. Rutten, G. Hoeks, and J. Verlijsdonk, "2SrO. $3Al_2O_3$:Eu^{2+} and 1.29(Ba,Ca)O, $6Al_2O_3$:Eu^{2+} Two new blue-emitting phosphors," J. Electrochem. Soc. **136**(7), 2119–2123 (1989).

23. D. Wang, M. Wang, and G. Lü, "Synthesis, crystal structure and X-ray powder diffraction data of the phosphor matrix $4SrO.7Al_2O_3$," J. Mater. Sci. **34**(20), 4959–4964 (1999).

24. D. Dutczak, T. Jüstel, C. Ronda, and A. Meijerink, "Eu^{2+} luminescence in strontium aluminates," Phys. Chem. Chem. Phys. **17**(23), 15236–15249 (2015).

25. F. Clabau, X. Rocquefelte, S. Jobic, P. Deniard, M.-H. Whangbo, A. Garcia, and T. Le Mercier, "Mechanism of phosphorescence appropriate for the long-lasting phosphors Eu^{2+}-doped $SrAl_2O_4$ with codopants Dy^{3+} and B^{3+}," Chem. Mater. **17**(15), 3904–3912 (2005).

26. J. Botterman, J. Joos, and P. F. Smet, "Trapping and detrapping in $SrAl_2O_4$:Eu,Dy persistent phosphors: Influence of excitation wavelength and temperature," Phys. Rev. B: Condens. Matter Mater. Phys. **90**(8), 085147 (2014).

27. G. Blasse and B. C. Grabmaier, *Luminescent Materials* (Springer-Verlag, 1994), p. 123.

28. J. M. Ngaruiya, S. Nieuwoudt, O. M. Ntwaeaborwa, J. J. Terblans, and H. C. Swart, "Resolution of Eu^{2+} asymmetrical emission peak of $SrAl_2O_4$:Eu^{2+}, Dy^{3+} phosphor by cathodoluminescence measurements," Mater. Lett. **62**(17-18), 3192–3194 (2008).

29. A. Shukla, "Development of a critically evaluated thermodynamic database for the systems containing alkaline-earth oxides," Thesis, University of Montreal, (2012).

30. V. Singh, J-J. Zhu, M. Tiwari, M. Soni, M. Aynayas, S-H. Hyun, R. Narayanan, M. Mohapatra, and V. Natarajan, "Characterization, luminescence and EPR investigations of Eu^{2+} activated strontium aluminate phosphor," J. Non-Cryst. Solids **355**(50-51), 2491–2495 (2009).

31. E. Cordoncillo, B. Julian-Lopez, M. Martinez, M. L. Sanjuán, and P. Escribano, "New insights in the structure–luminescence relationship of Eu:$SrAl_2O_4$," J. Alloys Compd. **484**(1-2), 693–697 (2009).

32. X. B. Yu, C. L. Zhou, X. H. He, X. F. Peng, and S. P. Yang, "The influence of some processing conditions on luminescence of $SrAl_2O_4$:Eu^{2+} nanoparticles produced by combustion method," Mater. Lett. **58**(6), 1087–1091 (2004).

33. S. H. Ju, S.G. Kim, J. C. Choi, H. L. Park, S.-I. Mho, and T. W. Kim, "Synthesis and characterization of white light emitting $Ca_xSr_{1-x}Al_2O_4$:Tb^{3+},Eu^{3+} phosphor for solid state lighting," Mater. Res. Bull. **34**(12-13), 1905–1909 (1999).

34. A. K. Prodjosantoso and B. J. Kennedy, "Synthesis and evolution of the crystalline phases in $Ca_{1-X}Sr_xAl_2O_4$," J. Solid State Chem. **168**(1), 229–236 (2002).

35. H. Pöllmann and R. Kaden, "X-ray investigations of solid solutions of monocalcium aluminate and monostrontium aluminate important phases in cement and phosphorescence materials," Powder Diffr. **29**(02), 141–146 (2014).

36. Q. Xie, B. Li, X. He, M. Zhang, Y. Chen, and Q. Zeng, "Correlation of structure, tunable colors, and lifetimes of (Sr, Ca, Ba)Al$_2$O$_4$:Eu^{2+}, Dy^{3+} phosphors," Materials **10**(10), 1198 (2017).

37. D. W. Goodwin and A.J. Lindop, "The crystal structure of CaO.2AI$_2$O$_3$," Acta Cryst. B **26**(9), 1230–1235 (1970).

38. M. Karmaoui, M.-G. Willinger, L. Mafra, T. Herntrich, and N. Pinna, "A general non-aqueous route to crystalline alkaline earth aluminate nanostructures," Nanoscale **1**(3), 360–365 (2009).

39. A. J. Lindop and D. W. Goodwin, "The refined structure of SrO.2A1$_2$0$_3$," Acta Cryst. B **28**(8), 2625–2626 (1972).

40. H. Boysen, M. Lerch, A. Stys, and A. Senyshyn, "Structure and oxygen mobility in mayenite (Ca$_{12}$Al$_{14}$O$_{33}$): a high-temperature neutron powder diffraction study," Acta Cryst. B **63**(5), 675–682 (2007).

41. R. D. Shannon, "Revised effective ionic radii and systematic studies of interatomic distances in halides and chalcogenides," Acta Cryst. A **32**(5), 751–767 (1976).

42. M. de Jong, L. Seijo, A. Meijerink, and F. T. Rabauw, "Resolving the ambiguity in the relation between Stokes shift and Huang–Rhys parameter," Phys. Chem. Chem. Phys. **17**(26), 16959–16969 (2015).

43. D. den Engelsen, P. G. Harris, T. G. Ireland, G. Fern, and J. Silver, "Symmetry-related transitions in the photoluminescence and cathodoluminescence spectra of nanosized cubic Y$_2$O$_3$:Tb^{3+}," ECS J. Solid State Sci. Technol. **4**(12), R145–R152 (2015).

44. D. den Engelsen, P. G. Harris, T. G. Ireland, G. Fern, and J. Silver, "Symmetry-Related Transitions in the Spectrum of Nanosized Cubic Y$_2$O$_3$:Tb^{3+}," ECS J. Solid State Sci. Technol. **4**(7), R105–R113 (2015).

45. L. Ning, X. Huang, Y. Huang, and P. A. Tanner, "Origin of Green Persistent Luminescence of Eu-Doped SrAl$_2$O$_4$ from Multiconfigurational *Ab Initio* Study of 4f^7 → 4f^{6}5d^1 Transitions," J. Mater. Chem. C **6**(25), 6637–6640 (2018).

46. J. Ueda, T. Nakanishi, Y. Katayama, and S. Tanabe, "Optical and optoelectronic analysis of persistent luminescence in Eu^{2+}-Dy^{3+} codoped SrAl$_2$O$_4$ ceramic phosphor," Phys. Status Solidi C **9**(12), 2322–2325 (2012).

47. M. Nazarov, M. G. Brik, D. Spassky, B. Tsukerblat, A. Nor Nazida, and M. N. Ahmad-Fauzi, "Structural and electronic properties of SrAl$_2$O$_4$:Eu^{2+} from density functional theory calculations," J. Alloys Compd. **573**(1), 6–10 (2013).

48. J. Ueda, T. Shinoda, and S. Tanabe, "Evidence of three different Eu^{2+} sites and their luminescence quenching processes in CaAl$_2$O$_4$:Eu^{2+}," Opt. Mater. **41**(1), 84–89 (2015).

49. J. Bierwagen, S. Yoon, N. Gartmann, B. Walfort, and H. Hagemann, "Thermal and concentration dependent energy transfer of Eu^{2+} in SrAl$_2$O$_4$," Opt. Mater. Express **6**(3), 793–803 (2016).

50. V. Vitola, D. Millers, K. Smits, I. Bite, and A. Zolotarjovs, "The search for defects in undoped SrAl$_2$O$_4$ material," Opt. Mater. **87**, 48–52 (2019).

51. D. den Engelsen, G. R. Fern, T. G. Ireland, P. G. Harris, P. R. Hobson, A. Lipman, R. Dhillon, P. J. Marsh, and J. Silver, "Ultraviolet and blue cathodoluminescence from cubic Y$_2$O$_3$ and Y$_2$O$_3$:Eu^{3+} generated in a transmission electron microscope," J. Mater. Chem. C **4**(29), 7026–7034 (2016).

52. D. den Engelsen, G. R. Fern, T. G. Ireland, and J. Silver, "Cathodoluminescence of Y$_2$O$_3$:Ln^{3+} (Ln = Tb, Er and Tm) and Y$_2$O$_3$:Bi^{3+} nanocrystalline particles at 200 keV," RSC Adv. **8**(1), 396–405 (2018).

53. M. Greger, M. Kollar, and D. Volhardt, "Isosbestic points: How a narrow crossing region of curves determines their leading parameter dependence," Phys. Rev. B **87**(19), 195140 (2013).

54. Y. Zorenko, T. Zorenko, T. Voznyak, A. Mandowski, Q. Xia, M. Batentschuk, and J. Friedrich, "Luminescence of F$^+$ and F centers in Al$_2$O$_3$-Y$_2$O$_3$ oxide compounds," IOP Conf. Ser.: Mater. Sci. Eng. **15**, 012060 (2010).

55. K. A. Denault, J. Brgoch, S. D. Kloß, M. W. Gaultois, J. Siewenie, K. Page, and R. Seshadri, "Average and Local Structure, Debye Temperature, and Structural Rigidity in Some Oxide Compounds Related to Phosphor Hosts," ACS Appl. Mater. Interfaces **7**(13), 7264–7272 (2015).